BIOCHEMISTRY
including biophysical chemistry & molecular biology

Article

pubs.acs.org/biochemistry

Examining Reaction Specificity in PvcB, a Source of Diversity in Isonitrile-Containing Natural Products

Jing Zhu,[†] Geoffrey M. Lippa,[‡] Andrew M. Gulick,[‡,§] and Peter A. Tipton*[,†]

[†]Department of Biochemistry, University of Missouri, Columbia, Missouri 65211, United States
[‡]Hauptman-Woodward Medical Research Foundation, Buffalo, New York 14203, United States
[§]Department of Structural Biology, University at Buffalo, Buffalo, New York 14203, United States

Supporting Information

ABSTRACT: Many bacteria produce isonitrile-containing natural products that are derived from aromatic amino acids. The synthetic clusters that control biosynthesis most commonly encode two enzymes, designated PvcA and PvcB, as well as additional enzymes that direct synthesis of the natural product. The PvcA enzyme installs the isonitrile moiety at the amino group of either tyrosine or tryptophan, as dictated by the particular pathway. The common pathway intermediate produced by PvcA is directed toward different ultimate products by PvcB, a member of the family of Fe^{2+}, α-ketoglutarate-dependent oxygenases. To continue our investigation of the structural and functional properties of the isonitrile biosynthetic pathways, we present here a study of the PvcB homologues from three organisms. Two pathways, derived from *Pseudomonas aeruginosa* and *Xenorhabdus nematophila*, produce known products. A third PvcB homologue from *Erwinia amylovora* is part of an uncharacterized pathway. Our results demonstrate the diversity of reactions catalyzed. Although all PvcB enzymes catalyze the hydroxylation of the tyrosine isonitrile substrate, the elimination of the hydroxyl in *Pseudomonas* and *Erwinia* is driven by deprotonation at Cα, resulting in the initial production of an unsaturated tyrosine isonitrile product that then cyclizes to a coumarin derivative. PvcB from *Xenorhabdus*, in contrast, catalyzes the same oxygenation, but loss of the hydroxyl group is accompanied by decarboxylation of the intermediate. Steady-state kinetic analysis of the three reactions and a docking model for the binding of the tyrosine isonitrile substrate in the PvcB active site highlight subtle differences between the PvcB homologues.

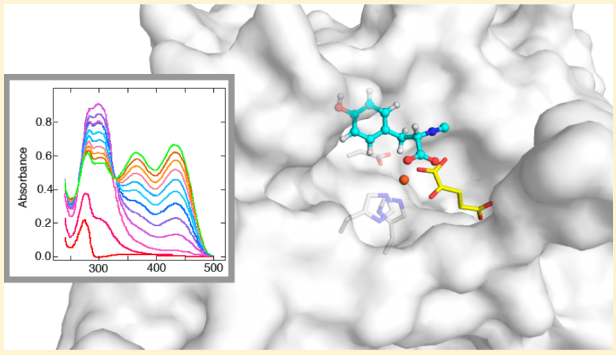

A wide variety of isonitrile-containing natural products has been identified from marine and terrestrial microorganisms. Alkaloids, terpenes, and amino acids are among the parent compounds that are modified to contain isonitriles, and biological activities include antibacterial and cytotoxic effects.[1,2] While attention has naturally focused on the origin of the isonitrile functionality, the remaining enzymes in the operon can diverge, resulting in a wide variety of natural products.[3] Most commonly, the synthetic operon contains a gene that is annotated as an Fe^{2+}, α-ketoglutarate-dependent oxygenase and is often labeled *pvcB*. The PvcA enzymes catalyze installation of the isonitrile moiety into either tyrosine or tryptophan. The PvcB oxygenases function downstream of the isonitrile synthase[4] and may be responsible for the chemical diversity of the products. Much effort has been devoted to unraveling the iron-dependent chemistry that leads to substrate hydroxylation in reactions catalyzed by enzymes within this family.[5]

The *pvc* operon of *Pseudomonas aeruginosa*, harboring four genes, was originally implicated in the maturation of the chromophore of the siderophore pyoverdine,[6,7] resulting in the use of *pvc* for pyoverdine chromophore in the names of these and homologous genes. Subsequent genetic analysis in *P. aeruginosa* showed that *pvc* mutants are still capable of pyoverdine production and growth under iron limitation,[8,9] casting doubt on the functional assignment of the *pvc* operon. Following the identification of an isonitrile derivative of tryptophan produced by a homologous gene cluster from an environmental DNA source,[4] characterization of the *P. aeruginosa pvc* operon demonstrated that the true biosynthetic product is paerucumarin (**2**), or 2-isocyano-6,7-dihydroxycoumarin,[3] which is derived from tyrosine. Paerucumarin does in fact share some features with the pyoverdine chromophore and was detected in its hydrated form in cultures of *pvc*-overexpressing cells.[7] Analysis of homologous proteins has demonstrated that PvcA catalyzes the installation of the isonitrile.[4] Only a few products of *pvc* biosynthetic operons have been chemically characterized,[3] including the glycosylated derivative rhabduscin (**3**), that is produced by *Xenorhabdus nematophila* (Scheme 1).

Received: March 9, 2015
Revised: April 9, 2015
Published: April 13, 2015

DOI: 10.1021/acs.biochem.5b00255
Biochemistry 2015, 54, 2659−2669

Scheme 1

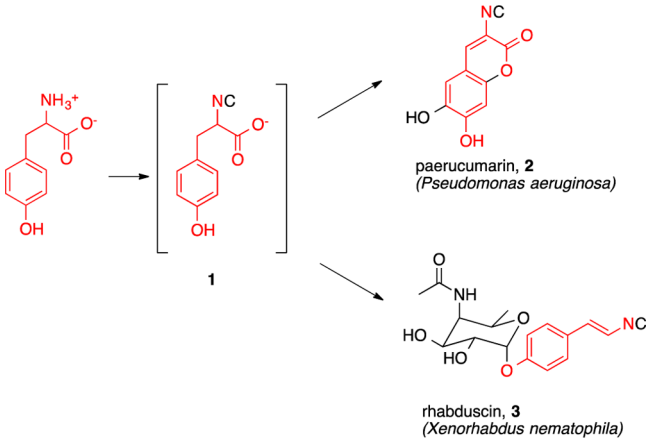

The amino acid sequence and the structure of *P. aeruginosa* PvcB suggest that it is an Fe^{2+}, α-ketoglutarate-dependent enzyme.[8] Similarly, a PvcB orthologue is found in the *X. nematophila* gene cluster responsible for rhabduscin synthesis.[10] Neither PvcB orthologue has been characterized biochemically, although the ultimate product from the enzymes encoded by the operon is known. We report here the reactions catalyzed by these PvcB enzymes. Additionally, a PvcB orthologue in an uncharacterized operon from *Erwinia amylovora*, a Gram-negative plant pathogen that causes fire blight in certain fruit trees, was also chosen for study on the basis of the differences in the operon organization, and to build a diverse pool of enzyme targets. The identification of the product of this cluster is being pursued separately. We have previously determined the structures of PvcA and PvcB from *P. aeruginosa* in the absence of ligands.[8] Subsequent efforts to grow crystals of PvcB with informative ligands were unsuccessful; however, a higher-resolution structure was obtained that is included herein and was used for molecular docking experiments. For the sake of simplicity, the enzymes from *P. aeruginosa*, *X. nematophila*, and *E. amylovera* will be termed PaPvcB, XnPvcB, and EaPvcB, respectively.

MATERIALS AND METHODS

Buffers and common biochemicals were purchased from Fisher Scientific or Sigma and were used without further purification. Organic solvents were stored over molecular sieves, and imidazole used in column chromatography was recrystallized from ethyl acetate.

Cloning of PvcB Genes. The cloning and construction of the expression vector for PaPvcB have been described previously.[8] The genes for XnPvcB and EaPvcB were synthesized commercially (Genewiz, Inc.); sequences encoding NdeI and XhoI restriction sites were incorporated at the 5′ and 3′ ends, respectively. Sequences of XnPvcB (WP_010845413.1) and EaPvcB (WP_004157574.1) were identified through an NCBI BLAST search originating from the PaPvcB sequence (AAC21672.1). The synthetic genes were subcloned into the pET-15bTEV plasmid. *Escherichia coli* 10G cells were transformed with the expression vectors and stored in 20% glycerol at −80 °C.

Expression and Purification of PaPvcB for Crystallization. The PaPvcB expression vector was used to transform *E. coli* BL21(DE3) cells. Transformants were selected by growth on LB plates containing carbenicillin. Individual colonies were picked and used to inoculate 10 mL cultures, which grew overnight at 37 °C, and were then used to inoculate flasks containing 1 L of LB medium supplemented with 100 μg/mL carbenicillin. The cultures were grown at 37 °C with rotary shaking (250 rpm) to an optical density of 0.4−0.6 and then placed on ice to lower the temperature to ∼16 °C. IPTG was added to a final concentration of 0.3 mM to induce recombinant protein expression, and the growth was continued at 16 °C for 16−20 h. The cells were harvested by centrifugation at 3993*g* for 20 min, yielding 4−5 g of cell paste per liter of medium. The cell paste was stored at −80 °C until it was needed. Frozen cell paste (typically 4−5 g) was suspended in 20 mL of buffer composed of 50 mM Tris (pH 7.5), 250 mM NaCl, 20 mM imidazole, and 0.2 mM TCEP. The suspension was kept on ice and mixed with 1 mg/mL lysozyme for 30 min. The cells were lysed by sonication, and the cell debris was removed by ultacentrifugation at 40000 rpm for 40 min. The clarified supernatant was loaded onto a 5 mL Ni-NTA column (GE HisTrap HP) pre-equilibrated in the same buffer that was used for lysing the cells and washed with 25 mL of buffer at a rate of 2 mL/min. A step gradient consisting of 65 mL of lysis buffer containing 50 mM imidazole, followed by 55 mL of lysis buffer with 300 mM imidazole, was used to elute the protein. The purity of the protein was assessed by SDS−PAGE, and the pooled protein fractions were dialyzed against 50 mM Tris (pH 7.5), 250 mM NaCl, and 0.2 mM TCEP. TEV protease (1 mg per 50 mg of target) was included with the sample during dialysis, to cleave the affinity tag. The protein was concentrated using an Amicon Ultra 10K MWCO centrifugation filter and loaded back onto the Ni-NTA column to remove the protease and cleaved tag. The flow-through sample was purified with a Superdex 200 size-exclusion column (GE HiLoad 16/600 Superdex 200 pg) using buffer containing 40 mM Tris (pH 7.5), 50 mM NaCl, and 0.2 mM TCEP, to remove contaminants. The single peak was concentrated to 5 mg/mL for crystallization. Protein concentrations were determined spectrophotometrically using an extinction coefficient of 40000 M^{-1} cm^{-1} at 280 nm.[8]

The expression and purification of XnPvcB and EaPvcB followed the same procedures that have been described for PaPvcB. The appropriate extinction coefficients were calculated from the amino acid sequences using ProtParam.[11]

Synthesis of Tyrosine Isonitrile, 1. Tyrosine isonitrile was synthesized by N-formylation of tyrosine, followed by dehydration of the *N*-formyl group with Burgess reagent.[12,13] L-Tyrosine (10 mmol, 1.8 g) was dissolved in formic acid (5 mL), and acetic formic anhydride[14] (40 mmol, 3.5 g) was added. The reaction vessel was capped with a drying tube and placed on ice for 4 h. The reaction was quenched by addition of 20 mL of water, and the solution was concentrated to dryness under reduced pressure. Ice-cold hydrochloric acid (1 N, 20 mL) was added to the residue to dissolve the remaining tyrosine. The product was collected by filtration and washed with water: ^{1}H NMR (DMSO-d_6) δ 7.96 (s, 1H), 7.07 (d, J = 8.4 Hz, 2H), 6.76 (d, J = 8.4 Hz, 2H), 4.43 (m, 1H), 2.94 (dd, J = 13.8, 5.0 Hz, 1H), 2.74 (dd, J = 13.8, 9.0 Hz, 1H).

Formyl tyrosine (1 mmol, 0.22 g) was methylated with trimethylsilyldiazomethane (5 mmol of a 2.0 M solution in diethyl ether) and MeOH (12 mmol) in dry dichloromethane (8 mL) at room temperature for 10 min.[15] The solvents were removed by rotary evaporation: ^{1}H NMR (DMSO-d_6) δ 7.98 (s, 1H), 6.99 (d, J = 6.6 Hz, 2H), 6.67 (d, J = 6.6 Hz, 2H), 4.51

DOI: 10.1021/acs.biochem.5b00255
Biochemistry 2015, 54, 2659−2669

(m, 1H), 3.61 (s, 3H), 2.93 (dd, J = 13.8, 5.7 Hz, 2H), 2.78 (dd, J = 13.8, 9.0 Hz, 2H).

The remaining residue (~1 mmol of formyl tyrosine methyl ester) was dissolved in dry dichloromethane (8 mL). Burgess reagent [(methoxycarbonylsulfamoyl)triethylammonium hydroxide, inner salt] (1 mmol, 0.24 g) was added and the solution heated to reflux for 2 h.[13] The product was purified by column chromatography using 50 g of silica gel equilibrated in $CHCl_3$. After the sample had been loaded, the column was washed with 100 mL of $CHCl_3$ and then 200 mL of a $CHCl_3$/MeOH mixture (98:2). Tyrosine isonitrile methyl ester eluted when the column was washed with 100 mL of the $CHCl_3$/MeOH mixture (97:3): ^{1}H NMR (DMSO-d_6) δ 7.03 (d, J = 8.4 Hz, 2H), 6.71 (d, J = 8.4 Hz, 2H), 5.02 (m, 1H), 3.73 (s, 3H), 3.08 (dd, J = 14.1, 5.0 Hz, 1H), 2.97 (dd, J = 14.1, 7.5 Hz, 1H).

The material from the previous step (~0.5 mmol) was dissolved in 1.5 mL of THF; 0.5 mL of 2.0 M LiOH was added, and the solution was incubated at room temperature for 16 h to hydrolyze the methyl ester. Attempts to desalt tyrosine isonitrile by anion exchange and size-exclusion chromatography resulted in hydration of the isonitrile group, so the solution was lyophilized and the product used without further purification: ^{1}H NMR (D_2O) (Figure S1 of the Supporting Information) δ 7.07 (d, J = 7.5 Hz, 2H), 6.98 (d, J = 7.5 Hz, 2H), 4.32 (m, 1H), 3.05−2.86 (m, 2H); ^{13}C NMR (D_2O) δ 172.8, 155.6 (isonitrile C), 153.1, 130.6, 127.3, 115.6, 60.9, 37.6; FT-IR (KBr pellet) 2170 cm^{-1} (isonitrile group).

PvcB Activity Assay. Activities of the purified PvcB proteins were evaluated in the presence of synthetic tyrosine isonitrile and the cosubstrates α-ketoglutarate and Fe^{2+}. All reactions were conducted under aerobic conditions at 25 °C. Typical assay mixes contained 200 μM tyrosine isonitrile, 100 μM α-ketoglutarate, 10 μM $(NH_4)_2Fe(SO_4)_2$, 50 mM HEPES (pH 7.8), 150 mM NaCl, and PvcB. The reactions were initiated by adding PvcB and were monitored spectrophotometrically at 240−500 nm. Scans of the reaction mixtures were acquired every 0.5 min for ~10 min at room temperature. Control reactions were performed by omitting one of the substrates or the enzyme from the reaction mixture. PvcB activities were also tested using formyl tyrosine or tyrosine in place of tyrosine isonitrile. In addition, the effects of ascorbic acid, TCEP, and dithiothreitol on the reactions were examined.

Kinetic Analysis. Steady-state kinetic assays were conducted in solutions containing 50 mM HEPES (pH 7.8), 150 mM NaCl, 10 μM $(NH_4)_2Fe(SO_4)_2$, 50 μM ascorbic acid, α-ketoglutarate (5−30 μM), and tyrosine isonitrile (5−50 μM), thermostated at 25 °C. Reactions were monitored using a Carey 50 Bio UV−vis spectrophotometer. Product formation was detected by the increase in absorbance at 310 nm for the XnPvcB reaction and at 360 nm for the PaPvcB and EaPvcB reactions. An extinction coefficient of 4300 M^{-1} cm^{-1} was used to convert the absorbance to product concentration in the XnPvcB reaction, and a value of 2885 M^{-1} cm^{-1} was used in the PaPvcB and EaPvcB reactions.

Data Analysis. Initial velocity kinetic data were fit to the appropriate functions using GraFit version 5.0 (Erithacus Software). In the following functions, A and B are the concentrations of α-ketoglutarate and tyrosine isonitrile, respectively, and K_a and K_b are their Michaelis constants. K_{ia} is the dissociation constant for α-ketoglutarate, and V is the maximal velocity. Equation 1 describes reactions that follow a steady-state sequential mechanism; eq 2 is for ping-pong mechanisms, and eq 3 is for rapid equilibrium ordered mechanisms.

$$v = \frac{VAB}{K_{ia}K_b + K_bA + K_aB + AB} \quad (1)$$

$$v = \frac{VAB}{K_bA + K_aB + AB} \quad (2)$$

$$v = \frac{VAB}{K_{ia}K_b + K_bA + AB} \quad (3)$$

Analysis of the product spectra obtained in the PaPvcB reaction utilized singular-value decomposition, as implemented in KinTek Explorer, version 4.0.[16] Details of the analysis are provided in the Supporting Information.

Reaction Product Identification. Large scale PvcB reactions were conducted in 2 mL solutions containing 10 mM tyrosine isonitrile, 10 mM α-ketoglutarate, 5 mM ascorbic acid, 0.5 mM $(NH_4)_2Fe(SO_4)_2$, and ~50 μM PvcB in 50 mM HEPES (pH 7.8) and 150 mM NaCl. The XnPvcB reaction mixture was incubated at room temperature for 2 h and then extracted with two 4 mL aliquots of ethyl acetate. The organic phases were combined, and the solvent was removed by rotary evaporation. The residue was dissolved in 600 μL of methanol-d_4 and analyzed by ^{1}H NMR spectroscopy. A sample of the ethyl acetate extract of the XnPvcB reaction mixture was also prepared in methanol and analyzed by LC−MS (described in detail in the Supporting Information). The PaPvcB and EaPvcB reactions were quenched 5 min after addition of the enzyme by introducing the methylating reagent TMS-CHN_2. The methylation reaction was performed by injecting 0.5 mL of the PvcB reaction solution into 2 mL of ethyl acetate containing 500 mM methanol and 250 mM TMS-CHN_2. The solution was vortexed for 10 min, and after the phases had separated, the organic phase was removed and evaporated to dryness. The residue was dissolved in 0.5 mL of methanol for LC−MS analysis. To detect the formation of succinate in the PvcB reactions, another large scale reaction was conducted, and after incubation at room temperature for 2 h, aliquots of $CHCl_3$ were added to denature the protein. Following removal of the enzyme by centrifugation, the remaining solution was passed through a short Chelex 100 (Bio-Rad) column to remove the Fe^{3+}. The flow-through was dried and dissolved in D_2O for ^{1}H NMR analysis.

Determination of the Structure of PaPvcB and Computational Modeling. Initial crystallization conditions were established by Drake and Gulick.[8] Using similar conditions, we grew multiple crystals in the presence of ligands or probed the crystals with soaking conditions; no density consistent with bound ligands was ever observed. A higher-resolution model that is used for molecular docking experiments is presented. Crystals around 200 μm × 200 μm were cryoprotected by being soaked for 10−15 min in mother liquor [0.1 M BTP (pH 7.5), 5% PEG 20000, and 0.1 M sodium citrate tribasic] with 34% glycerol. Data collection took place at beamline 23ID-B of the Advanced Photon Source (APS) using a MAR 300 detector. Data were indexed, integrated, and scaled with iMOSFLM and AIMLESS.[17] The PaPvcB structure was determined by molecular replacement using the protein atoms of Protein Data Bank (PDB) entry 3EAT. This model was subjected to iterative model building[18] and refinement with both REFMAC and PHENIX[19] using the native data to 2.05 Å resolution. The final model contains 2207 protein atoms, 150

DOI: 10.1021/acs.biochem.5b00255
Biochemistry 2015, 54, 2659−2669

waters, and three molecules of glycerol. The diffraction data statistics and refinement statistics are listed in Table 1.[17] The final coordinates and structure factors have been deposited in the PDB as entry 4YLM.

Table 1. Diffraction Data Statistics and Refinement Statistics of *Pa*PvcB

PDB entry	4YLM
beamline	APS 23-ID-B
wavelength (Å)	1.0323
space group	$P6_322$
unit cell dimensions [*a*, *b*, *c* (Å)]	125.0, 125.0, 107.2
no. of molecules per asymmetric unit	1
resolution range (Å)	40−2.0 (2.07−2.0)[a]
no. of observations	414157
no. of unique reflections	32890
multiplicity	12.6
completeness (%)	100 (100)[a]
$\langle I/\sigma \rangle$	12.6 (4.6)[a]
R_{merge} (%)	12.2 (53.8)[a]
R_{pim} (%)	5.0 (16.4)[a]
CC(1/2)	0.996 (0.925)
Refinement	
R_{factor} (%)	18.73 (21.03)[a]
R_{free} (%)	21.88 (22.18)[a]
no. of protein molecules/water atoms	2207/150
root-mean-square deviation for bond distances (Å)	0.007
root-mean-square deviation for bond angles (deg)	1.055
Wilson *B* factor (Å^2)	30.2
average *B* factor (Å^2)	
protein (all, main, side)	34.7, 33.4, 35.4
glycerol	47.8
solvent	37.0
Ramachandran analysis (%)	
favored	98.1
allowed	1.9
outliers	0
Molprobity ClashScore	4.82 (98th percentile)

[a]Values in parentheses are for the highest-resolution shell (2.07−2.02 Å for diffraction data and 2.11−2.05 Å for refinement).

Docking was performed with AutoDock Vina[20] and DOCK,[21] implemented through the Chimera suite of programs.[22] The PvcB protein was aligned with clavaminate synthase (PDB entry 1DRT) containing Fe^{2+}, α-ketoglutarate, and proclavaminic acid.[23] The Fe^{2+} and α-ketoglutarate were extracted from this file and incorporated into the PvcB structure, which served as the receptor for the docking. A search space surrounded the active site pocket with dimensions of 25 Å × 25 Å × 25 Å. The top docking poses were examined for score and positioning of the Cβ protons toward the iron atom and comparison to the site of hydroxylation within proclavaminic acid of PDB entry 1DRT.

RESULTS

Identification of the Substrates for PvcB Proteins. The synthesis of authentic tyrosine isonitrile, **1**, allowed us to test whether it was the correct substrate for the PvcB proteins. Spectroscopic analysis demonstrated dramatic spectral changes when each PvcB enzyme was incubated with tyrosine isonitrile, Fe^{2+}, and α-ketoglutarate under aerobic conditions (Figure 1). Control reactions lacking tyrosine isonitrile or α-ketoglutarate failed to show any spectral changes. Some turnover was observed in the absence of added Fe^{2+}; the extent of the reaction was stimulated by addition of ascorbate, suggesting that the enzyme is isolated with some Fe^{2+} bound. The PaPvcB reaction was explored using formyl-tyrosine in place of tyrosine isonitrile, and no reaction was observed. ^{1}H NMR spectroscopic analysis of competent reaction mixtures revealed that succinate was formed from α-ketoglutarate during the reaction. Thus, as predicted from the sequence and crystal structure of PaPvcB, the PvcB proteins are α-ketoglutarate-dependent enzymes.

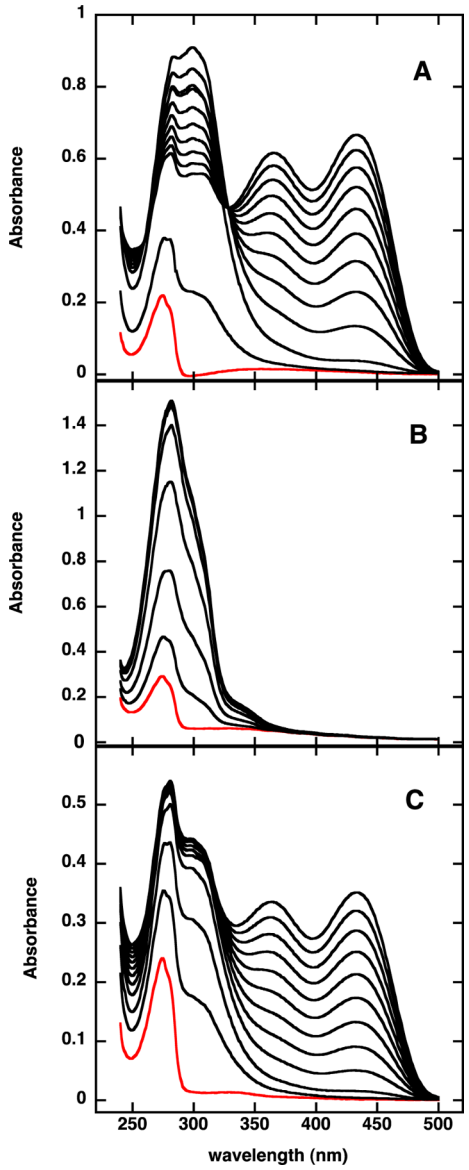

Figure 1. Spectroscopic changes during PvcB-catalyzed reactions. Each reaction mixture contained 200 μM tyrosine isonitrile, 100 μM α-ketoglutarate, 10 μM $(NH_4)_2Fe(SO_4)_2$, 150 mM NaCl, and 50 mM HEPES (pH 7.8). The spectrum acquired at time zero is colored red in each panel; subsequent spectra shown were acquired at 30 s and 1 min and then at 1 min intervals up to 10 min: (A) 0.46 μM PaPvcB, (B) 0.26 μM XnPvcB, and (C) 0.61 μM EaPvcB.

Identification of the Products of the PvcB Reactions. The spectral changes that accompanied the PaPvcB and EaPvcB reactions were more complex than those observed in the XnPvcB reaction, with a peak at 430 nm becoming

DOI: 10.1021/acs.biochem.5b00255
Biochemistry 2015, 54, 2659−2669

prominent at longer reaction times. When a relatively large amount of PaPvcB was utilized in the reaction, all of the tyrosine isonitrile was turned over within a few seconds, and the subsequent spectral changes were monitored. SVD analysis revealed that two species were predominant as the solution aged. Details of the analysis are provided in the Supporting Information. The reconstructed spectra of the two species are shown in Figure 2, and the extinction coefficients determined in the SVD analysis were used to calculate reaction velocities in the steady-state kinetic studies. The species whose maximal absorbance is at 280 nm is the true product of the PaPvcB reaction, and it decays nonenzymatically to the species with an absorbance peak at 430 nm.

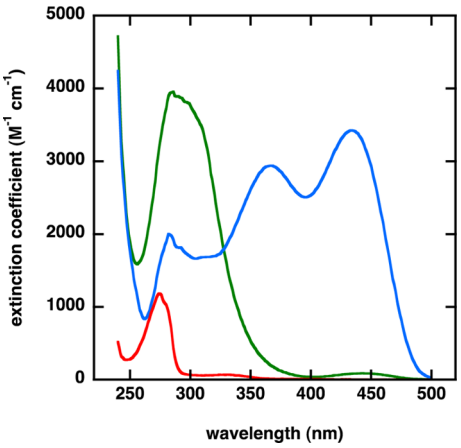

Figure 2. Component spectra of species in the reaction catalyzed by PaPvcB, determined by SVD analysis of time course spectra. The spectrum of the product of the PaPvcB reaction is colored green, and the spectrum of the species to which it decays nonenzymatically is colored blue. The spectrum of tyrosine isonitrile (red) is shown for comparison.

Identification of the products formed in each reaction from tyrosine isonitrile was achieved using ^{1}H NMR spectroscopy and LC−mass spectrometry. The XnPvcB product was stable and readily extracted into ethyl acetate, facilitating its identification. The ^{1}H NMR spectrum of the isolated product is shown in Figure 3 and has four aromatic protons that appear as doublets centered at 7.31 and 6.78 ppm (J = 9.0 Hz) and two doublets, each corresponding to one proton, centered at 6.96 and 6.45 ppm (J = 15.0 Hz). This matches the published spectrum of (*E*)-4-(2-isocyanovinyl)phenol, **5**.[3] The positive ion mass spectrum showed peaks at m/z 146.18, 164.05, and 178.10 (Figure 3). The low-mass peak is from isocyanovinylphenol; the second peak is either a water adduct or the product in which the isonitrile group has become hydrated, and the high-mass peak is presumed to arise from the methanol adduct of isocyanovinylphenol.

The instability of the product of the PaPvcB and EaPvcB reactions hindered its identification. Initial attempts to extract it into ethyl acetate failed, as did attempts to accumulate sufficient material for a ^{1}H NMR spectrum. When the reaction was quenched with a methylating reagent, however, the product was stabilized and rendered sufficiently hydrophobic to be extracted into organic solvent. LC−MS analysis of the PaPvcB and EaPvcB reactions yielded very similar results (Figure 4). A single species at m/z 204.0 was observed in each instance, which is assigned to 3-(4-hydroxyphenyl)-2-isocyanoacrylate

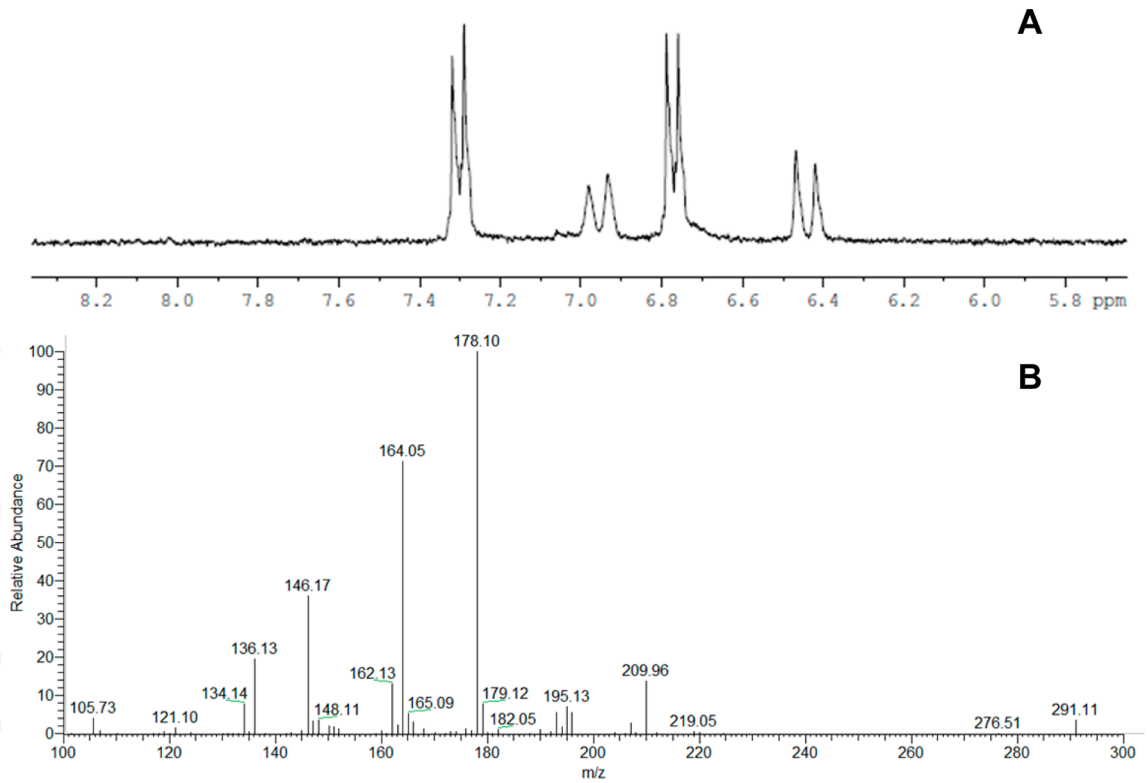

Figure 3. Identification of the product of the XnPvcB reaction. (A) For the ^{1}H NMR spectrum (MeOH-d_4 solvent), the reaction was conducted and the product isolated as described in the text. (B) Mass spectrum of the isolated product.

DOI: 10.1021/acs.biochem.5b00255
Biochemistry 2015, 54, 2659−2669

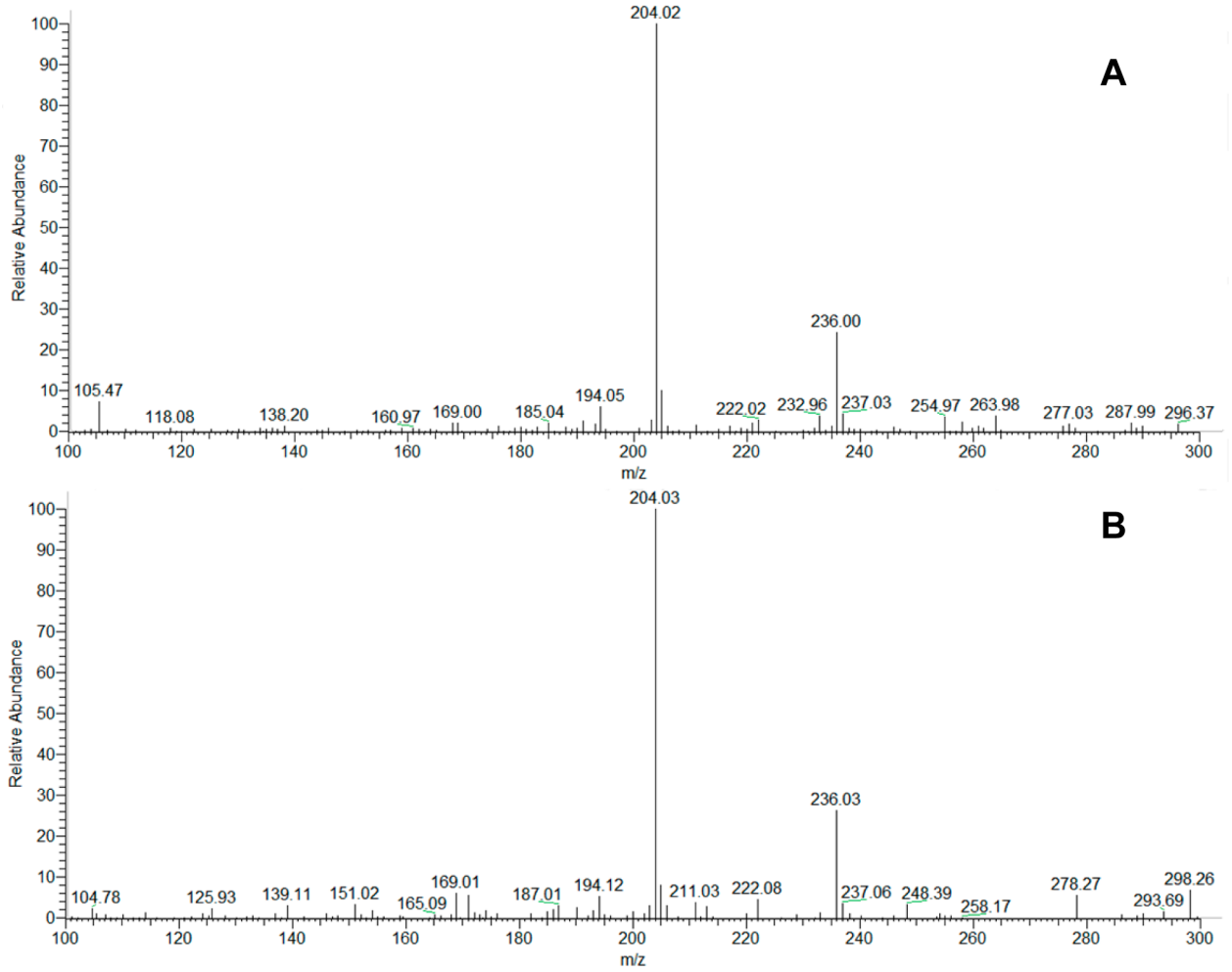

Figure 4. Mass spectra of products trapped by methylation of the (A) PaPvcB and (B) EaPvcB reactions.

methyl ester, indicating that the product of the PaPvcB and EaPvcB reactions is 3-(4-hydroxyphenyl)-2-isocyanoacrylate, **6**.

Steady-State Kinetic Characterization of PvcB Reactions. The steady-state kinetic parameters governing the reactions catalyzed by the three PvcB proteins characterized in this study are listed in Table 2. Complete kinetic characterization was not conducted, but the concentrations of α-ketoglutarate and tyrosine isonitrile were systematically varied. The data were visually inspected before being fit to the appropriate function. Interestingly, the double-reciprocal plots showed systematic differences that are often indicative of distinct kinetic mechanisms (Figure 5). The XnPvcB reaction yielded a family of lines intersecting to the left of the origin. The lines were parallel in the case of PaPvcB, and in the EaPvcB reaction, the lines intersected on the *y*-axis.

Table 2. Kinetic Parameters of PvcB Reactions

enzyme	k_{cat} (s^{-1})	K_m, α-ketoglutarate (μM)	K_m, tyrosine isonitrile (μM)
PaPvcB[a]	2.3 ± 0.2	23 ± 4	93 ± 15
XnPvcB[b]	5.1 ± 0.3	5.7 ± 1.1	13 ± 2
EaPvcB[c]	0.22 ± 0.01	4.8 ± 0.8	16 ± 2

[a]Kinetic parameters derived from a fit to eq 1. [b]Kinetic parameters derived from a fit to eq 2. [c]Kinetic parameters derived from a fit to eq 3.

High-Resolution Structure of PaPvcB and Molecular Docking. We have previously presented a crystal structure of PaPvcB.[8] We have continued to optimize crystals, partly in an attempt to identify the structure of the protein bound to substrates or substrate analogues. Despite numerous soaking and cocrystallization experiments with tyrosine, tyrosine isonitrile, iron, and α-ketoglutarate, none of the data sets that were collected and processed gave evidence of ligands in the PvcB active site. Through these efforts, however, a higher-resolution data set was collected. This structure is similar to the earlier structure, containing disordered loops at positions Asp99, Ser169−Tyr173, and Val200−Glu211. The least-squares displacement of the two structures, calculated for 270 Cα positions, is 0.2 Å. Although it is globally similar to the earlier structure, we used this higher-resolution structure for modeling and docking with the tyrosine isonitrile substrate.

Because we were unable to obtain crystals with protein bound to ligand, we used computational docking to identify a position for binding the substrate tyrosine isonitrile. We first aligned PaPvcB with homologous structures to identify the binding position of the iron and α-ketoglutarate. Ligand positions were taken from the structure of clavaminate synthase (PDB entry 1DRT). With these ligands fixed in the PaPvcB structure, we docked a molecule of tyrosine isonitrile.

Comparison of liganded structures of homologous proteins illustrates variation in the mode of substrate binding. We compared the docking poses from multiple runs with the

DOI: 10.1021/acs.biochem.5b00255
Biochemistry 2015, 54, 2659−2669

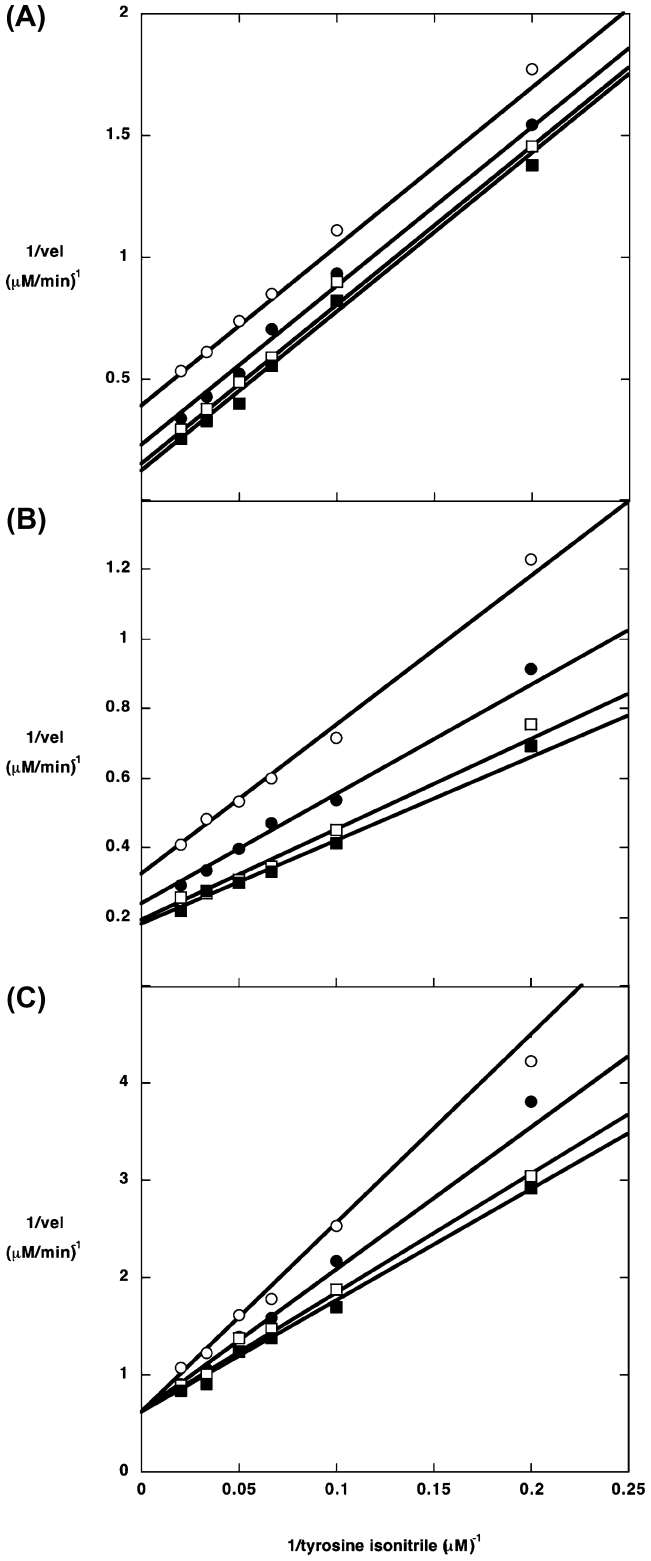

Figure 5. Double-reciprocal plots of the reactions catalyzed by PvcB enzymes. The concentration of tyrosine isonitrile was varied between 5 and 50 μM at (○) 5, (●) 10, (□) 20, and (■) 50 μM α-ketoglutarate. (A) PaPvcB, fit to eq 2. (B) XnPvcB, fit to eq 1. (C) EaPvcB, fit to eq 3.

structures of clavaminate synthase[23,24] and carbapenem synthase.[25] From the potential docking poses identified, one appeared to be most reasonable in terms of the free energy of binding and chemical plausibility (Figure 6). In this model, the aromatic ring of the ligand binds in a hydrophobic pocket formed by Met114, Tyr115, and Leu116, with potential contributions from Trp83, as well. The carboxyl group of the tyrosine isonitrile does not interact directly with any positively charged residues. Arg168 is present nearby at the start of a disordered loop and could interact with the carboxylate. The *pro-S* hydrogen from the Cβ position is directed toward the iron, potentially identifying the site of hydroxylation in the proposed PvcB mechanism. The distance from Cβ to the docked iron is 3.4 Å. Given the limitations of the accuracy from molecular docking, this distance is similar to 4.4 Å, the value observed for the distance between the iron and the analogous carbon atom in the clavaminate synthase substrate analogue *N*-acetyl arginine.[23] This structure (PDB entry 1DRY) contains a water molecule coordinated to the iron trans to the His259 equivalent residue. The pose of the docked tyrosine isonitrile is oriented such that hydroxylation at the *pro-S* position, and subsequent *anti* elimination upon abstraction of the α-proton, would result in the *E* configuration around the double bond, which is required for cyclization to form the coumarin ring in the PaPvcB-catalyzed reaction.

■ DISCUSSION

Paerucumarin, **2**, and rhabduscin, **3**, are examples of natural products derived from amino acids in which the amino group has been converted to an isonitrile. Paerucumarin appears to act as a signal molecule used by the bacteria to coordinate events in biofilm synthesis.[26] Rhabduscin is a potent inhibitor of insect phenoloxidase and plays a role in overcoming the innate immune system of insect hosts that the bacteria encounter.[27] In broad terms, both compounds are involved in intercellular communication; the abundance of microbial genomes that contain orthologues for the genes required for isonitrile synthesis suggests that many novel compounds or novel applications of known isonitrile-containing natural products remain to be recognized. Characterization of the biosynthetic enzymes involved will facilitate attempts to gain a deeper understanding of the biological roles of these compounds.

Operons that encode enzymes predicted to be involved in isonitrile metabolite synthesis have been identified on the basis of homology to a putative isonitrile synthase, e.g., IsnA or PvcA.[4,9] In each case, the operon also includes a gene encoding a putative α-ketoglutarate-dependent enzyme that is believed to act on the product of the isonitrile synthase reaction. In no instance has the activity of one of these enzymes been demonstrated. In this work, we have characterized the catalytic activity of three Fe^{2+}, α-ketoglutarate-dependent enzymes found in operons demonstrated or believed to be responsible for synthesis of isonitrile-containing metabolites in bacteria.

The crystal structure of PaPvcB revealed its similarity to known Fe^{2+}, α-ketoglutarate-dependent dioxygenases; however, no ligands were present in the structure that was determined, and the catalytic activity had not been tested.[8] Given that tyrosine isonitrile is the expected product of the PvcA reaction, it seemed reasonable to investigate whether tyrosine isonitrile was a substrate for PvcB. Dramatic spectroscopic changes were evident when the enzyme was incubated under aerobic conditions in the presence of tyrosine isonitrile, Fe^{2+}, and α-ketoglutarate. No change was observed in control reactions lacking tyrosine isonitrile or α-ketoglutarate; some activity was evident when Fe^{2+} was omitted, and the activity was enhanced by addition of ascorbate (data not shown). The stimulation of activity by ascorbate has been observed frequently in other

DOI: 10.1021/acs.biochem.5b00255
Biochemistry 2015, 54, 2659−2669

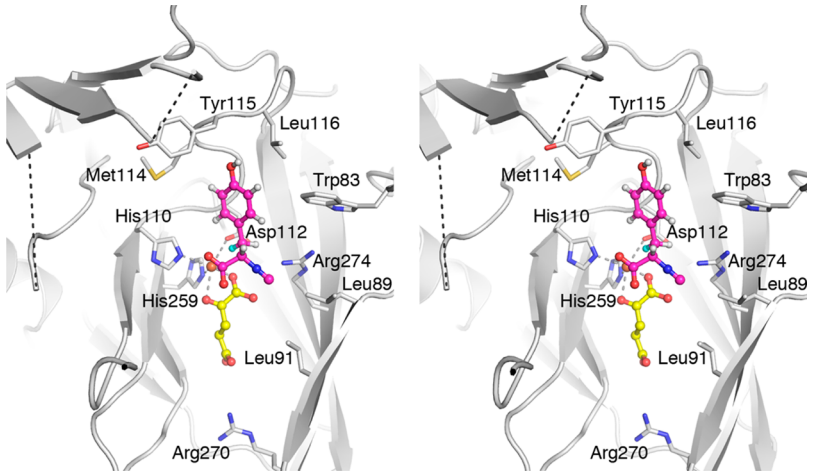

Figure 6. Stereorepresentation of the model of tyrosine isonitrile docked into the active site of PaPvcB. The Fe and α-ketoglutarate (yellow) from clavaminate synthase are included in the model. Tyrosine isonitrile is colored magenta; the *pro-S* hydrogen at Cβ is colored cyan. Disordered loops connecting Arg168 to Ser174 and Pro199 to Phe212 are shown with dashed lines.

Fe^{2+}, α-ketoglutarate-dependent dioxygenases.[28,29] PaPvcB was not active when tyrosine isonitrile was replaced in the reaction mixture with tyrosine or formyl-tyrosine. Finally, the assignment of PaPvcB as a member of the Fe^{2+}, α-ketoglutarate-dependent dioxygenase superfamily was confirmed by ^{1}H NMR spectroscopic analyses of samples, which clearly showed the conversion of α-ketoglutarate to succinate.

The more interesting question was the identity of the products formed from tyrosine isonitrile by each of the three enzymes. The XnPvcB reaction was spectroscopically distinct from the PaPvcB and EaPvcB reactions, and monitoring the reaction by HPLC and UV−visible spectroscopy indicated that the product was stable. ^{1}H NMR and mass spectrometric analyses were consistent with the assignment of the product as **5**, which arises from oxidative decarboxylation of tyrosine isonitrile. The natural product rhabduscin that is made by *X. nematophila* contains the isocyanovinylphenol moiety, so there is satisfying congruence between the *in vitro* XnPvcB reaction product and the final product of the metabolic pathway in which it participates.

Paerucumarin results from oxidative cyclization of tyrosine isonitrile, and the PaPvcB reaction yielded a species with absorbance at long wavelengths, as would be expected for a coumarin. However, close examination of reactions conducted with small amounts of enzyme revealed a lag in the appearance of the species that absorbed at long wavelengths; conducting the reaction with a large amount of enzyme showed that tyrosine isonitrile was rapidly converted to another species that did not absorb at long wavelengths but subsequently reacted to form the species distinguished by its absorbance peak at 430 nm. The time course of this conversion was monitored over the wavelength range from 240 to 400 nm, and singular-value decomposition was employed to deconvolute the spectra. In addition to determining the spectra of the components of the reaction solution, the SVD analysis revealed the kinetic relationship between them. The species that absorbed at 430 nm formed in a first-order reaction from another species characterized by an absorbance peak at 280 nm. In other words, PaPvcB converted tyrosine isonitrile into a relatively unstable species with maximal absorbance at 280 nm, which spontaneously decomposed into a compound with absorbance maxima at 360 and 430 nm.

The instability of the product of the PaPvcB reaction, and the fact that it could not be extracted into organic solvent, suggested that the carboxyl group in tyrosine isonitrile was still present. To generate sufficient material for characterization, a relatively large amount of PaPvcB was added to the substates, and the reaction was quenched within a few minutes by addition of trimethylsilyldiazomethane. Treatment of the reaction solution with the methylating agent both stabilized the product and rendered it capable of being extracted into ethyl acetate. We did not isolate enough material for ^{1}H NMR analysis, but mass spectrometry was consistent with identification of the esterified product as 3-(4-hydroxyphenyl)-2-isocyanoacrylate methyl ester. Thus, the product of the enzymatic reaction is **6**, formed by oxidation of tyrosine isonitrile.

The UV−visible spectroscopic properties of the EaPvcB reaction product were identical to those of the PaPvcB reaction product, as was its behavior on HPLC. Mass spectrometry was also consistent with the conclusion that the product (trapped as its methyl ester) was **6**. EaPvcB was identified by database mining, and the product of the pathway in which it operates is unknown. The gene is found in an operon along with a *pvcA* homologue and an open reading frame that is annotated as a flavin-dependent monooxygenase. It seems likely, then, that the product of the pathway will prove to derive from oxidative cyclization of the PvcB product. Of the PvcB orthologues characterized in this work, the two that are present in operons without a glycosyltransferase catalyze decarboxylation of tyrosine isonitrile. XnPvcB catalyzes decarboxylation of tyrosine isonitrile, and rhabduscin, the product of the pvc operon in *X. nematophila*, is the glycosyl conjugate of the PvcB product. Similarly, byelyankacin is a natural product isolated from *Enterbacter* sp. B20; it contains the same isocyanovinylphenol moiety as rhabduscin and is also glycosylated. It will be interesting to determine whether the correlation between PvcB reaction specificity and glycosylation of the pathway product holds as more *pvc* operons are characterized.

Fe^{2+}, α-ketoglutarate-dependent dioxygenases typically catalyze hydroxylation of unactivated alkyl C−H bonds or aromatic rings. The mechanisms of these reactions are the subject of several excellent reviews.[5,30] However, the products of the PvcB reactions characterized here are not hydroxylated. Scheme 2

DOI: 10.1021/acs.biochem.5b00255
Biochemistry 2015, 54, 2659−2669

Scheme 2

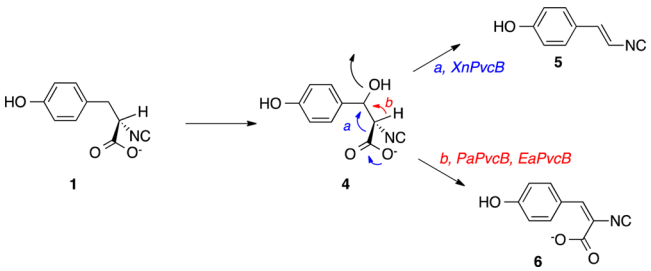

illustrates how the paradigmatic reaction can be applied to explain formation of the observed products. Hydroxylation at Cβ of tyrosine isonitrile generates an intermediate **4** that is common to all PvcB's. The different products arise from different ways that the hydroxyl group is expelled. In the XnPvcB reaction, decarboxylation at Cα drives the hydroxyl group to leave. In the PaPvcB and EaPvcB reaction, the expulsion of the hydroxyl group is caused by abstraction of a proton from the α-carbon. Since no atom from molecular oxygen is found in the tyrosine isonitrile-derived product of the PvcB reaction, strictly speaking, the enzymes are not dioxygenases, but consideration of the underlying reaction mechanism clearly demonstrates their place in the superfamily.

The arrangement of tyrosine isonitrile shown in Figure 6 emerged from docking studies and satisfies regiochemical and stereochemical constraints. Cβ is in the proximity of the Fe^{2+} atom, making hydroxylation of that position feasible. Further, hydroxylation at the *pro-S* position would result in an intermediate that yields **6**. Formation of the *E* isomer is required, so that the carboxyl group is positioned appropriately for cyclization to form the coumarin product. That the *pro-S* position is hydroxylated is a testable hypothesis, which we propose on the basis of the observation that enzyme-catalyzed dehydrations that involve abstraction of a proton α to a carboxylate typically undergo *anti* elimination.[31]

The sequences of PaPvcB and EaPvcB are 56% identical; XnPvcB is 42% identical with PaPvcB and 41% identical with EaPvcB. Only PaPvcB has been characterized structurally. We analyzed the docked model of tyrosine isonitrile in the context of sequence comparison. The residues of PaPvcB that form the pocket for the aromatic group in the docked model are conserved with the exception of Leu116, which is replaced with an Arg in XnPvcB. Arg168 of PaPvcB that is partly disordered in the structure is positioned near the carboxylate in the docked model. This arginine is conserved in EaPvcB and replaced with a threonine in XnPvcB. Although we note the presence of arginine and lysine before and after this threonine residue in XnPvcB, this difference may be partly responsible for the differences in the PvcB reactions catalyzed by these different enzymes. These changes, both involving differences in positively charged residues, may be partly responsible for differences in the enzyme active site that dictate differences in activity between PaPvcB and XnPvcB.

The mechanisms proposed in Scheme 2 require all three enzymes to have an active site general acid to facilitate expulsion of the hydroxyl group from Cβ in compound **4**. We note that residues Ser169−Tyr173 and Val200−Glu211 are disordered in the structure of PaPvcB. Neither loop is especially well-conserved; however, all three proteins carry an aspartic acid residue homologous to Asp203 of PaPvcB that could be important. A survey of 582 PvcB homologues through the TrEMBL database shows that this aspartic acid is present in more than half the members of the family.

The apparently different steady-state kinetic mechanisms exhibited by the three enzymes were unexpected. The K_m values for tyrosine isonitrile vary <10-fold and those for α-ketoglutarate <5-fold. However, the kinetic patterns for PaPvcB, XnPvcB, and EaPvcB were those typically seen for ping-pong, sequential, and rapid equilibrium ordered reactions, respectively. Because it is unlikely that these enzymes operate by fundamentally different mechanisms, it is worth exploring how the observed kinetic patterns could arise. Examination of eqs 1−3 reveals that eq 1 is the most general, in the sense that it contains all the terms also found in eq 2 or 3. The rapid equilibrium ordered kinetic pattern described by eq 3 and exhibited by EaPvcB is observed when the K_aB term is absent. This occurs when the binding and dissociation of α-ketoglutarate are rapid compared to the rest of the catalytic cycle; that is, its binding effectively comes to equilibrium. In terms of the kinetic mechanism shown in Figure 5, the rapid equilibrium ordered pattern is observed when k_5 or k_7 is much smaller than the other rate constants. In fact, k_{cat} for EaPvcB is lower than that of the other reactions, although it is not known whether chemistry or product release is rate-limiting. The sequential pattern observed in the XnPvcB reaction indicates that all the terms in the denominator of eq 1 contribute significantly to the velocity, and the pattern is a family of lines that intersect to the left of the *y*-axis. The ping-pong pattern exhibited by PaPvcB would seem to indicate a kinetic mechanism that is distinct from those of the other two enzymes, but as has been mentioned previously,[32] seemingly parallel patterns in double-reciprocal plots can arise in sequential mechanisms when the experimental data lack sufficient precision to detect small slope effects, which are contributed by the $K_{ia}K_b$ term in the denominator of the rate equation. In this instance, the slope effects will tend to zero when the dissociation constant for α-ketoglutarate is much smaller than its K_m. In an ordered bi-bi sequential mechanism, the dissociation constant for the first substrate is k_2/k_1 and the K_m is $(k_5k_7)/[k_1(k_5 + k_7)]$. Thus, when chemistry or product release is rapid relative to the preceding steps, the term in the velocity equation that introduces the slope effect can become very small and the double-reciprocal plots will approximate a family of parallel lines. These interpretations of the steady-state kinetics data will be evaluated by transient-state kinetic investigations to pinpoint the rate-limiting portions of the reaction cycles in the three enzymes.

The explosion of sequence information has allowed the virtual exploration of the metabolic capabilities of myriad organisms. However, the difficulties presented by misannotation in databases are widely recognized, and verifying the predictions of protein function that are suggested by synteny and sequence remains important. In this case, the PvcB proteins were correctly assigned as Fe^{2+}, α-ketoglutarate-dependent oxygenases, but it remained necessary to identify the products of the catalytic reactions in the laboratory. The unique properties of XnPvcB, which cause it to catalyze decarboxylation of its substrate, were not evident from sequence analysis alone and, in fact, remain to be identified; however, as more PvcB proteins are experimentally characterized, the sequence signatures that are correlated with particular chemical transformations should become evident.

DOI: 10.1021/acs.biochem.5b00255
Biochemistry 2015, 54, 2659−2669

■ ASSOCIATED CONTENT

Supporting Information

Additional methods and Figures S1−S4. This material is available free of charge via the Internet at http://pubs.acs.org.

Accession Codes

Coordinates have been deposited in the Protein Data Bank as entry 4YLM.

■ AUTHOR INFORMATION

Corresponding Author

*E-mail: tiptonp@missouri.edu. Fax: 573-882-5635. Telephone: 573-882-7968.

Funding

This research was supported by a grant from the National Science Foundation (MCB 1158169 to A.M.G. and P.A.T.).

Notes

The authors declare no competing financial interest.

■ ACKNOWLEDGMENTS

We thank Professor Timothy Glass (Department of Chemistry, University of Missouri) for helpful discussions.

■ ABBREVIATIONS

BTP, 1,3-bis[tris(hydroxymethyl)methylamino]propane; HEPES, *N*-(2-hydroxyethyl)-*N*′-(2-ethane)sulfonic acid; HPLC, high-performance liquid chromatography; IPTG, isopropyl β-D-1-thiogalactopyranoside; LC−MS, liquid chromatography−mass spectrometry; MWCO, molecular weight cutoff; NMR, nuclear magnetic resonance; NTA, nitrilotriacetic acid; SDS−PAGE, sodium dodecyl sulfate−polyacrylamide gel electrophoresis; SVD, singular-value decomposition; TCEP, tris(2-carboxyethyl)phosphine; TMS-CHN_2, (trimethylsilyl)-diazomethane.

■ REFERENCES

(1) Micallef, M. L., Sharma, D., Bunn, B. M., Gerwick, L., Viswanathan, R., and Moffitt, M. C. (2014) Comparative analysis of hapalindole, ambiguine and welwitindolinone gene clusters and reconstitution of indole-isonitrile biosynthesis from cyanobacteria. *BMC Microbiol. 14*, 213.

(2) Scheuer, P. J. (1992) Isocyanides and cyanides as natural products. *Acc. Chem. Res. 25*, 433−439.

(3) Brady, S. F., Bauer, J. D., Clarke-Pearson, M. F., and Daniels, R. (2007) Natural Products from isnA-Containing Biosynthetic Gene Clusters Recovered from the Genomes of Cultured and Uncultured Bacteria. *J. Am. Chem. Soc. 129*, 12102−12103.

(4) Brady, S. F., and Clardy, J. (2005) Cloning and Heterologous Expression of Isocyanide Biosynthetic Genes from Environmental DNA. *Angew. Chem. 44*, 7063−7065.

(5) Krebs, C., Galonić Fujimori, D., Walsh, C. T., and Bollinger, J. M. (2007) Non-Heme Fe(IV)−Oxo Intermediates. *Acc. Chem. Res. 40*, 484−492.

(6) Stintzi, A., Cornelis, P., Hohnadel, D., Meyer, J.-M., Dean, C., Poole, K., Kourambas, S., and Krishnapillai, V. (1996) Novel pyoverdine biosynthesis gene(s) of *Pseudomonas aeruginosa* PAO. *Microbiology 142*, 1181−1190.

(7) Stintzi, A., Johnson, Z., Stonehouse, M., Ochsner, U., Meyer, J.-M., Vasil, M. L., and Poole, K. (1999) The *pvc* Gene Cluster of *Pseudomonas aeruginosa*: Role in Synthesis of the Pyoverdine Chromophore and Regulation by PtxR and PvdS. *J. Bacteriol. 181*, 4118−4124.

(8) Drake, E. J., and Gulick, A. M. (2008) Three-dimensional Structures of *Pseudomonas aeruginosa* PvcA and PvcB, Two Proteins Involved in the Synthesis of 2-Isocyano-6,7-dihydroxycoumarin. *J. Mol. Biol. 384*, 193−205.

(9) Clarke-Pearson, M. F., and Brady, S. F. (2008) Paerucumarin, a New Metabolite Produced by the pvc Gene Cluster from *Pseudomonas aeruginosa*. *J. Bacteriol. 190*, 6927−6930.

(10) Crawford, J. M., Kontnik, R., and Clardy, J. (2010) Regulating Alternative Lifestyles in Entomopathogenic Bacteria. *Curr. Biol. 20*, 69−74.

(11) Gasteiger, E., Hoogland, C., Gattiker, A., Duvaud, S., Wilkins, M. R., Appel, R. D., and Bairoch, A. (2005) Protein Identification and Analysis Tools on the ExPASy Server. In *The Proteomics Handbook* (Walker, J. M., Ed.) Humana Press, Totowa, NJ.

(12) Burgess, E. M., Penton, H. R., and Taylor, E. A. (1973) Thermal reactions of alkyl N-carbomethoxysulfamate esters. *J. Org. Chem. 38*, 26−31.

(13) Hemantha, H. P., and Sureshbabu, V. V. (2010) Isoselenocyanates derived from amino acid esters: An expedient synthesis and application to the assembly of selenoureidopeptidomimetics, unsymmetrical selenoureas and selenohydantoins. *J. Pept. Sci. 16*, 644−651.

(14) Muramatsu, I., Murakami, M., Yoneda, T., and Hagitani, A. (1965) The formylation of amino acids with acetic formic anhydride. *Bull. Chem. Soc. Jpn. 38*, 244−246.

(15) Leggio, A., Liguori, A., Perri, F., Siciliano, C., and Viscomi, M. C. (2009) Methylation of α-amino acids and derivatives using trimethylsilyldiazomethane. *Chem. Biol. Drug Des. 73*, 287−291.

(16) Johnson, K. A., Simpson, Z. B., and Blom, T. (2009) Global Kinetic Explorer: A new computer program for dynamic simulation and fitting of kinetic data. *Anal. Biochem. 387*, 20−29.

(17) Winn, M. D., Ballard, C. C., Cowtan, K. D., Dodson, E. J., Emsley, P., Evans, P. R., Keegan, R. M., Krissinel, E. B., Leslie, A. G., and McCoy, A. (2011) Overview of the CCP4 suite and current developments. *Acta Crystallogr. D67*, 235−242.

(18) Emsley, P., and Cowtan, K. (2004) Coot: Model-building tools for molecular graphics. *Acta Crystallogr. D60*, 2126−2132.

(19) Adams, P. D., Afonine, P. V., Bunkóczi, G., Chen, V. B., Davis, I. W., Echols, N., Headd, J. J., Hung, L.-W., Kapral, G. J., and Grosse-Kunstleve, R. W. (2010) PHENIX: A comprehensive Python-based system for macromolecular structure solution. *Acta Crystallogr. D66*, 213−221.

(20) Trott, O., and Olson, A. J. (2010) AutoDock Vina: Improving the speed and accuracy of docking with a new scoring function, efficient optimization, and multithreading. *J. Comput. Chem. 31*, 455−461.

(21) Lang, P. T., Brozell, S. R., Mukherjee, S., Pettersen, E. F., Meng, E. C., Thomas, V., Rizzo, R. C., Case, D. A., James, T. L., and Kuntz, I. D. (2009) DOCK 6: Combining techniques to model RNA−small molecule complexes. *RNA 15*, 1219−1230.

(22) Yang, Z., Lasker, K., Schneidman-Duhovny, D., Webb, B., Huang, C. C., Pettersen, E. F., Goddard, T. D., Meng, E. C., Sali, A., and Ferrin, T. E. (2012) UCSF Chimera, MODELLER, and IMP: An integrated modeling system. *J. Struct. Biol. 179*, 269−278.

(23) Zhang, Z., Ren, J., Stammers, D. K., Baldwin, J. E., Harlos, K., and Schofield, C. J. (2000) Structural origins of the selectivity of the trifunctional oxygenase clavaminic acid synthase. *Nat. Struct. Mol. Biol. 7*, 127−133.

(24) Zhang, Z., Ren, J.-s., Harlos, K., McKinnon, C. H., Clifton, I. J., and Schofield, C. J. (2002) Crystal structure of a clavaminate synthase−Fe(II)−2-oxoglutarate−substrate−NO complex: Evidence for metal centered rearrangements. *FEBS Lett. 517*, 7−12.

(25) Clifton, I. J., Doan, L. X., Sleeman, M. C., Topf, M., Suzuki, H., Wilmouth, R. C., and Schofield, C. J. (2003) Crystal structure of carbapenem synthase (CarC). *J. Biol. Chem. 278*, 20843−20850.

(26) Qaisar, U., Luo, L., Haley, C. L., Brady, S. F., Carty, N. L., Colmer-Hamood, J. A., and Hamood, A. N. (2013) The *pvc* Operon Regulates the Expression of the *Pseudomonas aeruginosa* Fimbrial Chaperone/Usher Pathway (Cup) Genes. *PLoS One 8*, e62735.

(27) Crawford, J. M., Portmann, C., Zhang, X., Roeffaers, M. B. J., and Clardy, J. (2012) Small molecule perimeter defense in

DOI: 10.1021/acs.biochem.5b00255
Biochemistry 2015, 54, 2659−2669

entomopathogenic bacteria. *Proc. Natl. Acad. Sci. U.S.A. 109*, 10821−10826.
(28) Myllylä, R., Majamaa, K., Günzler, V., Hanauske-Abel, H. M., and Kivirikko, K. I. (1984) Ascorbate is consumed stoichiometrically in the uncoupled reactions catalyzed by prolyl 4-hydroxylase and lysyl hydroxylase. *J. Biol. Chem. 259*, 5403−5405.
(29) Saari, R. E., and Hausinger, R. P. (1998) Ascorbic Acid-Dependent Turnover and Reactivation of 2,4-Dichlorophenoxyacetic Acid/α-Ketoglutarate Dioxygenase Using Thiophenoxyacetic Acid. *Biochemistry 37*, 3035−3042.
(30) Simmons, J. M., Müller, T. A., and Hausinger, R. P. (2008) Fe II/α-ketoglutarate hydroxylases involved in nucleobase, nucleoside, nucleotide, and chromatin metabolism. *Dalton Trans.*, 5132−5142.
(31) Schwab, J. M., Klassen, J. B., and Habib, A. (1986) Stereochemical course of the hydration reaction catalysed by β-hydroxydecanoylthioester dehydrase. *J. Chem. Soc., Chem. Commun.*, 357−378.
(32) Ning, J., Purich, D. L., and Fromm, H. J. (1969) Studies on the Kinetic Mechanism and Allosteric Nature of Bovine Brain Hexokinase. *J. Biol. Chem. 244*, 3840−3846.

DOI: 10.1021/acs.biochem.5b00255
Biochemistry 2015, 54, 2659−2669